

Transport and coarsening of gold nanoparticles in an orogenic deposit by dissolution–reprecipitation and Ostwald ripening

E. C. G. Hastie ^{1,2} , M. Schindler³, D. J. Kontak¹ & B. Lafrance ¹

The role of nanoparticle gold in the formation of gold deposits has long been debated. Evidence in support of this process is generally limited to epithermal-, Carlin- and seafloor massive-sulfide-type deposits where gold nanoparticles are associated with primary fluid related processes. At the Kenty orogenic deposit in Ontario, Canada, gold has been remobilized from early pyrite through secondary coupled dissolution-reprecipitation processes to form high-grade gold external to pyrite. Here we report gold nanoparticles and related textures that help document this gold coarsening process. A combination of focused ion beam technology and transmission electron microscopy provides a rare glimpse of gold coarsening frozen in time, which includes nanoparticles trapped in iron oxides and rutile and non-oriented attachment of gold nanoparticles to bulk gold suggesting coarsening via Ostwald ripening. The processes documented are applicable to orogenic deposits formed through Earth's history, and may explain the formation of ultra high-grade ore zones.

¹ Mineral Exploration Research Centre, Harquail School of Earth Sciences, Laurentian University, Sudbury, ON, Canada. ² Earth Resources and Geoscience Mapping Section, Ontario Geological Survey, Sudbury, ON, Canada. ³ Department of Geological Sciences, University of Manitoba, Winnipeg, MB, Canada. email: evan.hastie@ontario.ca

Orogenic Au deposits represent one of the most important Au resources on the planet, particularly those formed in Archean terranes^{1,2}. As the name suggests, these epigenetic deposits formed during collisional orogeny³ and, regardless of age and setting, are known for spectacular high-grade ore zones with coarse gold^{1,4–6}. There is, however, a growing recognition that the formation of such high-grade coarse gold is difficult to explain using conventional Au-in-solution processes^{4–7}. This has therefore catalyzed in recent years increased scrutiny of other possible mechanisms, such as Au enrichment via nanoparticle processes, to account for the formation of coarse gold^{5,6,8–10}.

The aqueous transport of primary gold nanoparticles has for some time been shown to be a factor in high-grade, “bonanza-type” gold ore zones in epithermal deposits^{8,10,11} and thus may also be a factor in forming high-grade gold in other deposit types^{5,6,9,11–15}. However, until now documenting gold nanoparticles as part of Au remobilization owing to secondary processes, as in orogenic deposits, has not been demonstrated. To do so is important, as it would show that such processes are also important for upgrading ore zones versus being exclusive to primary processes.

Geological setting, the Kenty Au deposit, and Au remobilization. The Abitibi greenstone belt (AGB) is one of the most Au endowed Archean terranes in the world and accounts for a significant portion of the total Au endowment in the Superior Province of Canada¹⁶. The Swayze area, which is the southwestern extension of the AGB (Fig. 1), contains volcanic and plutonic rocks with a wide range of compositions (ultramafic to felsic) as well as metasedimentary rocks (both chemical and clastic). These rocks were deposited and emplaced between ca. 2750 Ma and 2670 Ma^{17,18}. Metamorphosed rocks in the western AGB attained temperatures of 350–450 °C and maximum pressures of ~3 kbar (10 km depth) during the final construction of

the Superior Craton at ca. 2670 Ma to 2640 Ma¹⁹. Although metamorphosed, the prefix “meta” is herein omitted from the rock names for simplicity.

The Kenty orogenic Au deposit (Fig. 1) is located in the central part of the Swayze area. It was discovered in the 1930s and is characterized by high-grade ore zones with coarse gold. Kenty is an excellent natural laboratory to study Au remobilization processes because it has a simple mineralization history and has escaped the multitude of overprinting events that complicate the interpretation of ore-forming processes in many orogenic deposits⁴. The Au mineralization is hosted in altered pillow basalts and granitoid rocks⁴, the latter dated at 2684.7 ± 1.5 Ma (U–Pb zircon). Two generations of Au mineralization are present: (1) early Au in pyrite localized to ankerite alteration zones marginal (i.e., <1–2 m) to quartz veins; and (2) later coarse gold lining fractures that cut the quartz veins⁴. The late coarse gold commonly lines conjugate fractures that formed in the hinge of the folded quartz veins with microfolded gold-rutile intergrowths in the wallrocks of the veins⁴.

Our previous research⁴ has interpreted the late coarse gold at Kenty to be a product of remobilization from earlier pyrite based on: (1) textures indicative of dissolution–reprecipitation processes²⁰ that increase towards the quartz veins hosting coarse gold. These textures reflect the destruction of primary chemical zonation, porosity development, and the formation of secondary inclusions (e.g., native gold, sulfides, and tellurides) consistent with trace elements (e.g., Au, Ag, Te, Cu) enriched in the primary zones; (2) SEM-EDS (energy dispersive spectroscopy) imaging and laser ablation inductively coupled mass spectrometry (LA-ICP-MS) elemental mapping of pyrite that shows progressive loss of Au and associated elements commensurate with the degree of pyrite modification and its proximity to quartz veins; (3) elements that are spatially associated with Au in pyrite (e.g., Ag, Cu, Te) are also associated with, and incorporated into, late coarse gold phases exterior to pyrite (e.g., Cu and Ag in native gold, petzite, hessite, calaverite); and (4) the Au content of

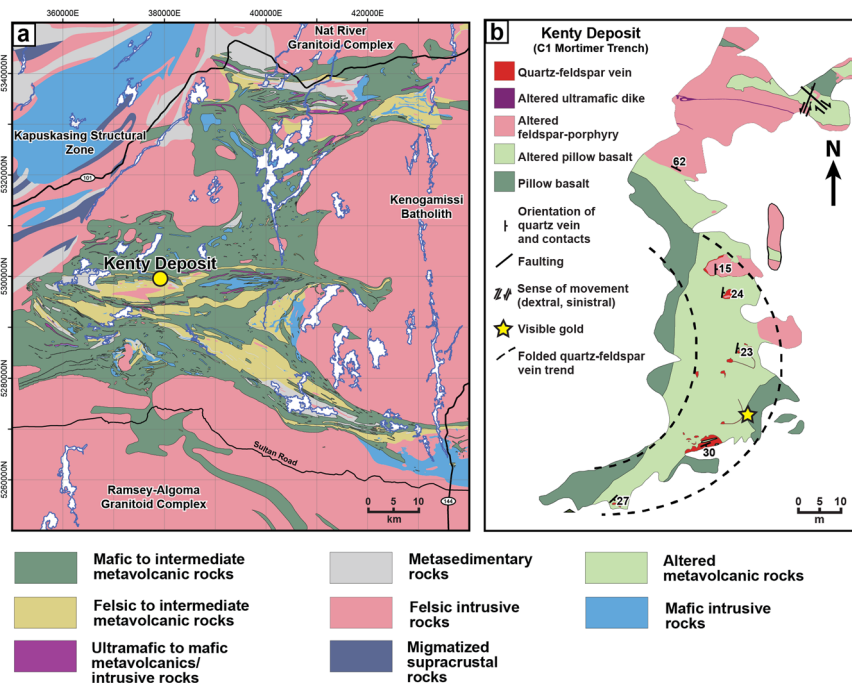


Fig. 1 Location and geologic maps of the Swayze area and Kenty deposit. **a** Simplified geologic map of the Swayze area, southwestern Abitibi greenstone belt. Location information provided as Universal Transverse Mercator (UTM) co-ordinates using North American Datum 1983 (NAD83) in Zone 17.

b Geologic outcrop map of the C1 Mortimer trench at the Kenty deposit. All maps are modified from previous Ontario Geological Survey and Society of Economic Geologists, Inc. publications^{4,47,48}.

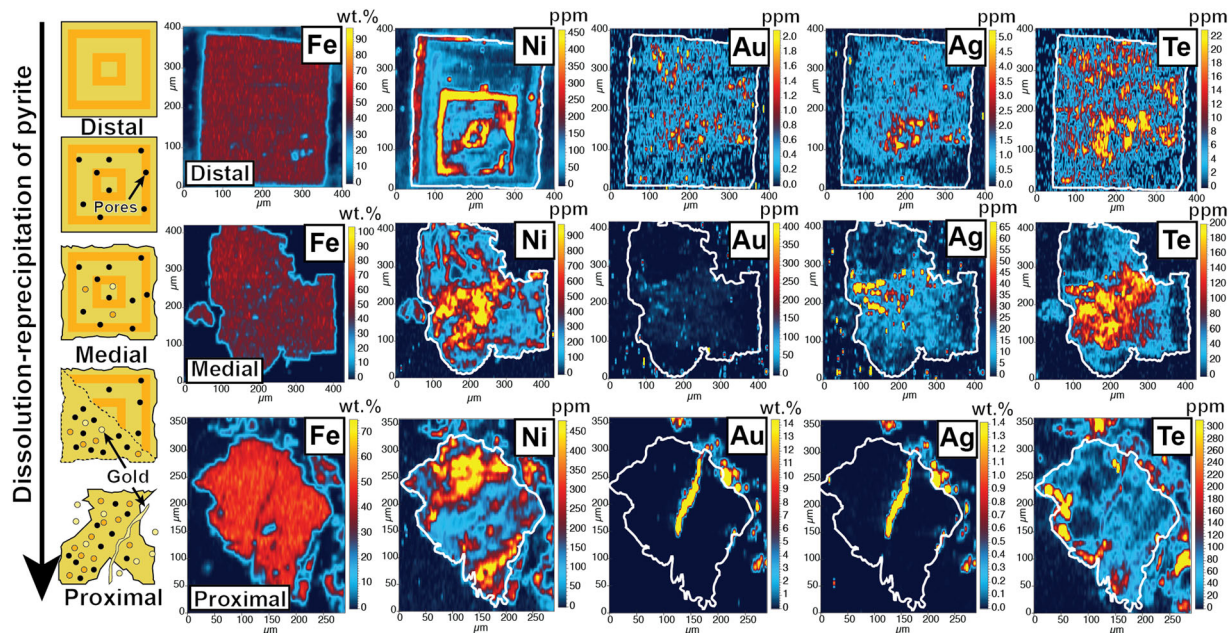


Fig. 2 Summary of dissolution–precipitation and Au remobilization at the Kenty deposit (modified from previous research in Society of Economic Geologists, Inc. publication⁴). Schematic diagram of dissolution–precipitation textures in relation to LA-ICP-MS elemental maps for Fe, Ni, Au, Ag, and Te for distal, medial and proximal pyrite. Increasing pyrite modification highlights textures consistent with dissolution–precipitation²⁰ and Au remobilization from pyrite⁴. Au gold, Ag silver, Fe iron; Ni, nickel; Te, tellurium.

primary pyrite (i.e., 100 s to 1000 s ppm) is sufficient to account for abundance of coarse gold hosted in late fractures⁴. A summary of this dissolution–precipitation model (Fig. 2) highlights the progressive loss of Au from pyrite with its increasing textural and chemical modification.

This research further demonstrated that the liberated Au from pyrite was likely remobilized at temperatures as low as 335 °C via fluid-mediated polymetallic melts enriched in low melting point chalcophile elements (LMCE), such as Te^{4,21–26}. Indeed, a number of recent studies provide substantive evidence to support Au concentration by LMCE-rich melts in the presence of a fluid^{24,25}. Seemingly enigmatic are areas at the Kenty deposit, as with many Au deposits worldwide, where zones hosting coarse gold lack evidence for LMCE-rich phases. We previously suggested that LMCE-rich melts may operate in conjunction with nanoparticle transport to account for Au upgrading at the Kenty deposit⁴, but we only provided evidence for the former mechanism. Thus, convincing evidence for the presence of gold nanoparticles in this Archean orogenic Au setting remains to be demonstrated.

Results and discussion

Gold nanoparticles, associated mineral phases, and textures.

Here, we report on the occurrence of gold nanoparticles within samples from the high-grade ore assemblage at the Kenty Au deposit (Fig. 1). To demonstrate this, we chose a mineralized sample (Fig. 3a–d) with evidence of Au remobilization⁴. The sample contains early-stage auriferous pyrite (\approx 800 ppm Au) in spatial association with late-stage coarse gold. Sample sections were extracted from a thin section by focused ion beam-scanning electron microscopy and thinned to foils for subsequent transmission electron microscopy (TEM) studies. The foils were extracted from the interior of the above-described pyrite grain and across its interface with gold-hematite-albite-rutile grains (Fig. 3d).

TEM examination of the FIB section from the interior of the pyrite (Supplementary Fig. 1) indicates the presence of nano-size Au-Ag-Te-Pb domains with droplet-like morphologies (Fig. 3e, f). The spatial overlap of Au-Ag-Te in the droplet suggests a telluride

phase (e.g., petzite); as Pb is concentrated toward the upper part of the droplet it may be part of another phase (altaite?). In addition to the droplets, bright sub-nanometer-size domains in the pyrite (Fig. 3e, f) and LA-ICP-MS elemental maps of pyrite grains (Fig. 2; distal and medial) also suggest that finely dispersed elemental Au, Ag, and Te occur throughout the pyrite.

The FIB section extracted along the pyrite margin (Fig. 3d) contains gold surrounded by grains of Fe oxide, pyrite, albite, and rutile (Fig. 4). On the lower left side of the FIB section, a large grain of Fe oxide is in contact with pyrite (Fig. 4a, b). This Fe oxide grain also connects to Fe-oxides on the margins of gold, albite and rutile and is also in the interior of the latter two minerals (Fig. 4b). The Fe-oxides are present prior to extraction (Fig. 3d) and thinning (Fig. 4b, c) and remain throughout the thinning process even when the gap in the area between gold and albite widens (Fig. 4d).

The larger Fe oxide grain (Fig. 4a, b) is composed of intergrown hematite, goethite, and magnetite/maghemite (Fig. 5a, b) and it contains gold nanoparticles ranging in size from 1 to 5 nm (Fig. 5c–e). A portion of the Fe oxide on the margin of gold that was previously attached to the larger Fe oxide grain (Fig. 4) is composed of hematite (Fig. 5f, g). This hematite also contains gold nanoparticles that range in size from 1 to 5 nm (Fig. 5h–j).

Observing the Fe oxide between the gold and albite (Fig. 4), a thin layer (5–10 nm thick) of the Fe oxide remained after FIB thinning on the gold surface. This thin layer contains gold nanoparticles whose lattice orientation is different from that of the coarse gold (Fig. 6a–c).

The Fe oxide filling that occurs between the gold and rutile grain boundary (Fig. 4a, b) also contains gold nanoparticles. At the far end of this grain boundary, gold nanoparticles up to 10 nm in size occur within rutile in close proximity to the gold surface (Fig. 6d–f).

Discussion on gold nanoparticles and their chemical behavior.

Documenting the nature and origin of gold nanoparticles in an Archean orogenic deposit (i.e., Kenty) is an important step towards understanding how high-grade ore zones form in such

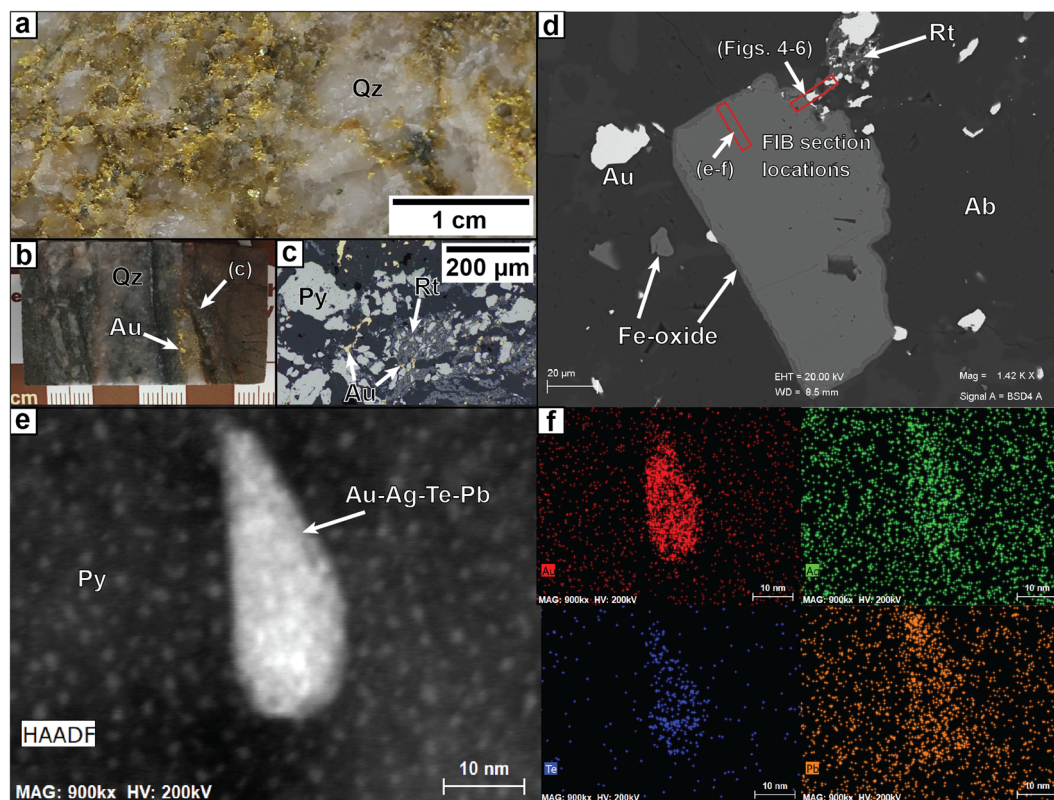


Fig. 3 Hand specimen, SEM, and STEM-EDS images of gold and associated mineral phases. **a** Gold in quartz from the Kenty deposit, Swayze area, Ontario (Sample M17410). Photo taken with the permission of the Royal Ontario Museum (ROM); sample number refers to the ROM sample catalog. **b** Gold in quartz sample from the Kenty deposit used in this study. **c** Reflected light image of porous pyrite, native gold, and rutile. Native gold crosscuts pyrite and is intergrown with rutile. **d** SEM backscattered electron image of Au-bearing pyrite, native gold, and associated minerals with FIB section locations shown with red rectangles. **e** STEM image of nano-size Au-bearing polymetallic phase with droplet-like morphology hosted in the pyrite shown in **d**. **f** STEM-EDS element maps of Au, Ag, Te, and Pb for image shown in **e**. Ab albite, Ag silver Au gold, Fe iron, Pb lead, Py pyrite, Qz quartz, Rt rutile, Te tellurium. Some images have been cropped and rotated to highlight specific features.

Au deposits in general given that most previous research on this topic is restricted to epithermal, Carlin, and seafloor massive-sulfide deposits^{8–10,12,13}. Although mechanisms have been suggested for nanoparticle aggregation previously^{8,10}, evidence for nanoparticle processes related to secondary remobilized gold has been lacking until now. The following discussion aims to resolve some of these aspects.

Caution must be exercised when preparing samples by FIB milling since redeposition of material is possible²⁷ and some TEM observations may be equivocal (e.g., Supplementary Fig. 2). Although this is a possibility, the gold nanoparticles presented in Figs. 3, 5, 6 are interpreted to be natural based on the following evidence: (1) separate and distinct gold nanoparticles are found in pyrite (Fig. 3e, f), Fe-oxides (Fig. 5) and rutile (Fig. 6d–f) with three-dimensional features that confirm that the gold nanoparticles are not surface redeposition; (2) pyrite, Fe oxide, and rutile also have an association with gold at the micro-scale (Fig. 3c, d)⁴; (3) the Fe oxide was present at the margin of gold and adjacent to pyrite (Fig. 4a–c) from the very beginning of the FIB sample thinning; (4) the gap in the FIB section widened during the FIB milling process, hence material was being removed and not added during this process (Fig. 4); (5) the Fe oxide between gold and albite narrowed during the FIB milling process (Fig. 4b–d), reinforcing the first two points; and (6) the Fe-oxides adjacent to pyrite and on the margin of gold include goethite, hematite, and magnetite/maghemite, as confirmed by selected area electron diffraction (SAED; Fig. 5a, b). A combination of Fe²⁺, Fe³⁺, and hydrous Fe-oxides within the same

assemblage would simply not form at the same time as redeposition during FIB milling, which precludes this being an artifact of the process.

Model on the formation, transport, and coarsening of gold nanoparticles. An oxidizing fluid was responsible for the dissolution-precipitation of pyrite at the Kenty deposit (Figs. 2, 3c, d)⁴. Once Au supersaturates in a fluid^{6,8–10}, gold nanoparticles would remain suspended in solution as long as their surface charges create larger net repulsive forces than net attractive forces. This phenomenon is best explained by Derjaguin-Landau-Verwey-Overbeek theory²⁸, which is commonly used to predict nanoparticle behavior, although quantum effects for particles <20 nm have yet to be resolved²⁹.

The surface charge of any nanoparticle is mainly affected by pH and counter-ion activity, although particle size and compositional variations (e.g., fluctuating Ag content of gold) can also affect the surface charge^{28,29}. Gold nanoparticles generally have a negative charge in near neutral to basic solutions and a positive one in highly acidic solutions^{10,30–32} with gold aggregation initiated where the pH favors a point of zero charge (PZC). The PZC for gold at 25 °C occurs at a pH of ≈3; however, no data currently constrains the PZC for gold at conditions relevant to ore deposit formation.

Two alternative models can explain the charge-dependent transport and coarsening of gold nanoparticles at the Kenty deposit based on the evidence presented above and the aforementioned summary of current research on nanoparticle

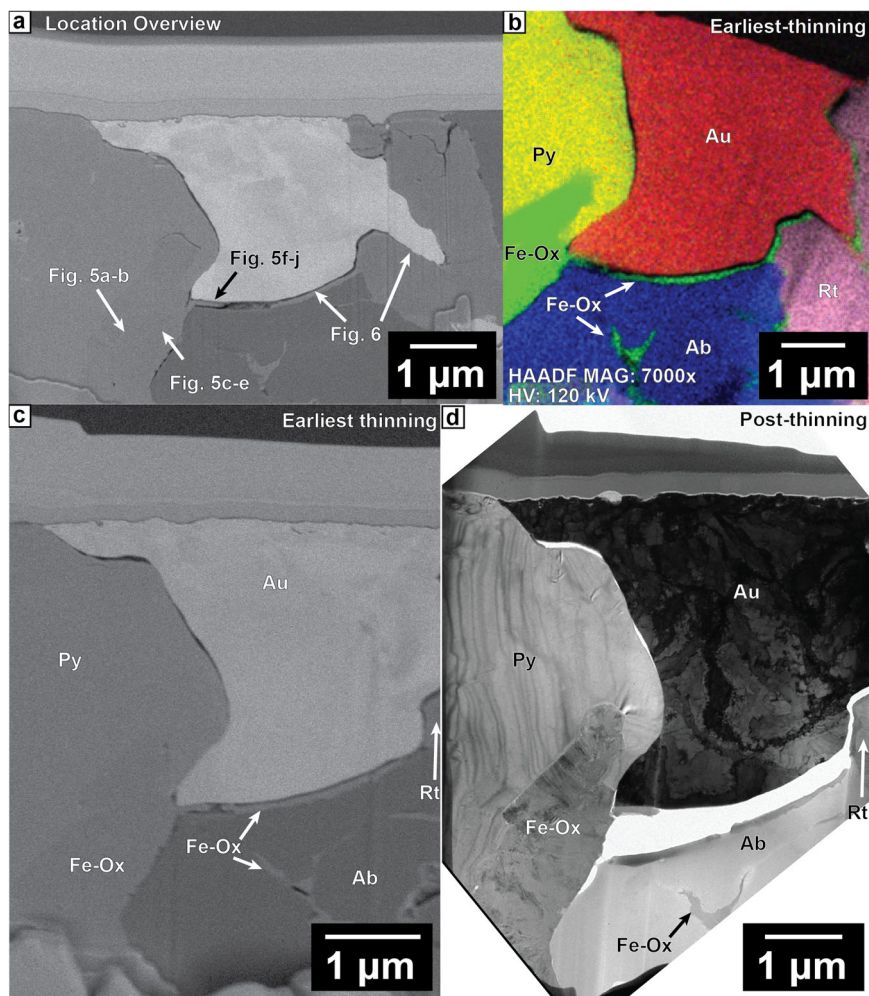


Fig. 4 SEM/TEM images and STEM-EDS phase map for the FIB section from the location shown in Fig. 3d. **a** SEM backscattered electron image of entire FIB section showing locations for Figs. 5 and 6. **b** STEM-EDS phase map highlighting different minerals shown in **a**. **c-d** SEM backscattered electron image showing FIB section at earliest stage of thinning and TEM image showing FIB section after thinning. *Ab* albite, *Au* gold, *Fe* iron, *Hem* hematite, *Ox* oxide, *Py* pyrite, *Rt* rutile. Some images have been cropped and rotated or reflected to produce similar orientations and aid comparison.

behavior. Dissolution of the early auriferous pyrite by an oxidizing fluid liberated Au (Fig. 2) and lowered the pH of the transporting fluid such that:

- (1) A fluid with a pH below the PZC of gold would promote the transport of positively charged gold nanoparticles. The dissolution of another phase (e.g., plagioclase) would be required to raise the pH of the fluid close to the PZC of gold to promote aggregation. This represents an intriguing mechanism, as both transport and aggregation of the gold nanoparticles are promoted by the dissolution of minerals. Albitization is a common process in Au deposits^{1,3,33} and Kenty is no exception⁴, as indicated by likely dissolution of original plagioclase (~An₃₀) based on the presence of end-member albite with associated alteration phases now seen (i.e., pyrite-muscovite(sericite)-carbonate)⁴.
- (2) A fluid with a pH above the PZC of gold would promote the transport of negatively charged gold nanoparticles. Adsorption of counter-ions, such as Fe³⁺ aqueous species (dominant under acidic to near-neutral pH conditions) on the surface of the gold nanoparticles, would have canceled their negative charge and thus promoted gold attachment and coarsening. This is a reasonable model

given the replacement of Au-rich pyrite by Fe-oxides (Fig. 3d) that contain gold nanoparticles (Figs. 5, 6a–c).

Recent studies on epithermal deposits have provided evidence for diffusion-limited gold aggregation resulting in “fractal” dendrites⁸. These textures form through oriented attachment of gold nanoparticles, but data from the Kenty deposit only shows non-oriented attachment (Fig. 6a). Thus, gold coarsening most likely occurred through a different mechanism.

Studies on nanoparticle attachment^{34,35} have provided evidence for crystallization of minerals via non-oriented attachment of nanoparticles. These studies showed that when non-oriented attachment occurs near flat or negatively curved surfaces, nanoparticles dissolve and a net transfer of monomers to the larger crystal occurs (i.e., Ostwald ripening)^{34,35}. Thus, the non-oriented attachment observed at Kenty (Fig. 6a) supports an interpretation whereby gold coarsened through the dissolution of gold nanoparticles and the mass transfer of Au monomers to the coarse gold lattice. The implication of this conclusion is that non-oriented attachment and Ostwald ripening may play an important role in the coarsening of gold in orogenic deposits. This also offers an alternative for gold coarsening by oriented attachment reported in epithermal environments⁸.

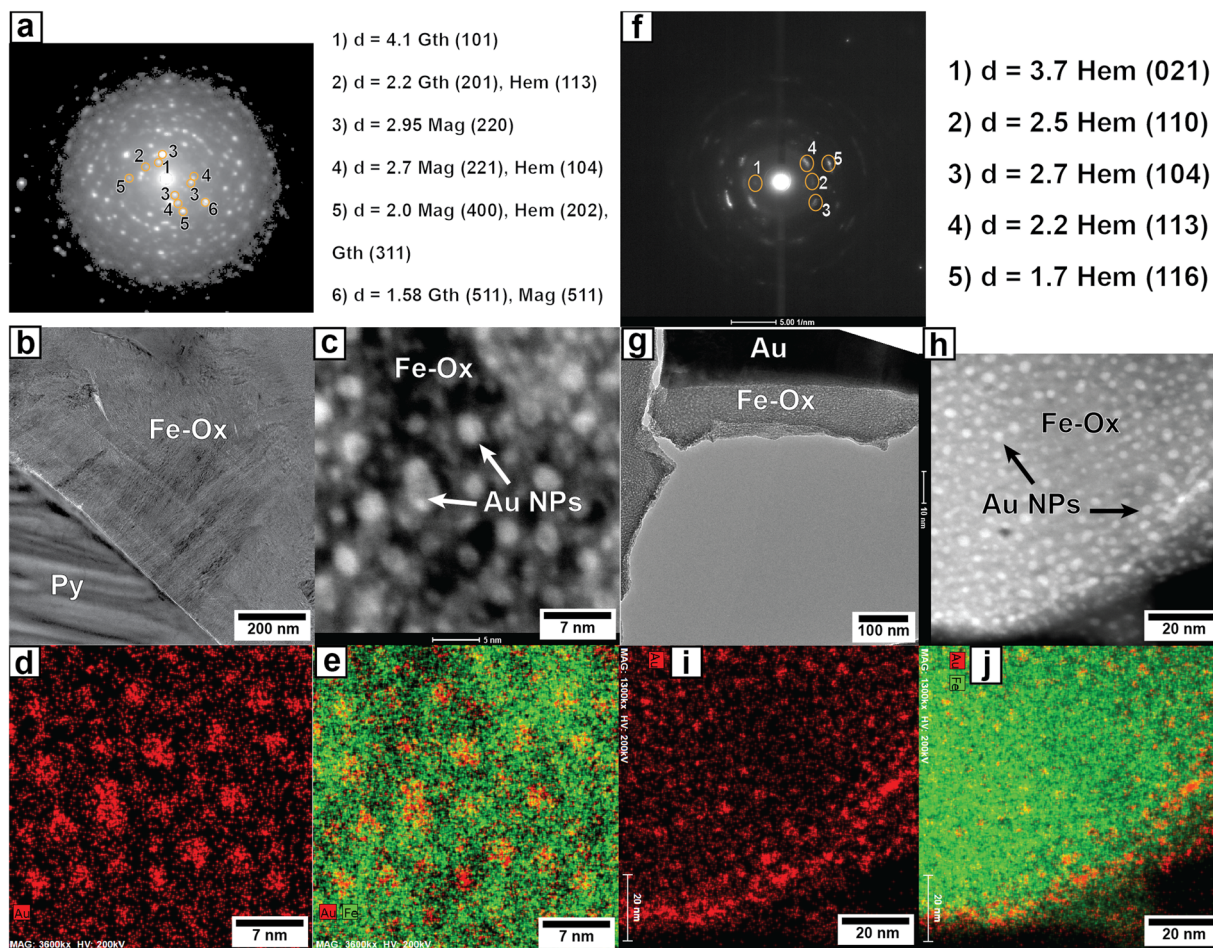


Fig. 5 SAED patterns, STEM/TEM images, and STEM-EDS elemental maps of Fe-oxides from locations shown in Fig. 4a. **a** SAED pattern for Fe-oxides (hematite, magnetite/maghemite, goethite) shown in **b**. Numbers and circles refer to diffraction legend. **b** TEM image of Fe-oxides in contact with pyrite. **c** STEM image of gold nanoparticles in Fe oxide. **d–e** STEM-EDS elemental maps highlighting gold nanoparticles within Fe-oxides from **c**. Au is in red, Fe in green. **f** SAED pattern for Fe oxide (hematite) shown in **g**. Numbers and circles refer to diffraction legend. **g** TEM image of Fe oxide in contact with gold. **h** STEM image of gold nanoparticles in Fe oxide. **i–j** STEM-EDS elemental maps highlighting gold nanoparticles within Fe oxide from **h**. Au is in red, Fe in green. Au gold, Fe iron, Hem hematite, Mag magnetite/maghemite, NP nanoparticle, Ox oxide. Some images have been cropped and rotated or reflected to produce similar orientations and aid comparison.

There is only a limited understanding of gold nanoparticle behavior in natural systems owing to the changing properties of minerals at the nanoscale and different nanoparticle-host-interactions³⁶. For example, the melting temperature of gold decreases dramatically from 1064 °C to <400 °C for isolated nanoparticles <3 nm^{13,37–39}, but becomes unpredictable for nanoparticles <2 nm where quantum effects need to be considered. In addition, the thermal stability of gold nanoparticles is also governed by their host mineral^{13,36}. In isolation, gold nanoparticles are stable until they reach the size-dependent melting curve^{37–39}, but in arsenian pyrite it has been shown that gold nanoparticles <4 nm in diameter would be unstable at temperatures relevant to orogenic deposits (i.e., 250–400 °C), and would coarsen through solid-state Ostwald ripening to become stable¹³. Assuming As does not greatly affect the stability of gold nanoparticles¹³, then the minimum temperatures obtained at the Kenty deposit (335 °C)⁴ would indicate that gold nanoparticles within pyrite would need to be a minimum of 4 nm to be stable¹³. However, gold nanoparticles between 1 and 5 nm in diameter occur in Fe-oxides indicating that this type of matrix affects the thermal stability of gold nanoparticles differently than pyrite. Thus, our observations (Figs. 5, 6) offer rare evidence of nanoparticles trapped prior to their coarsening into larger gold domains.

Considering that LMCE and Au can form a polymetallic melt in the presence of a fluid^{24,25} and that we have evidence at Kenty for polymetallic melt formation from the previous research⁴, as well as droplet-like polymetallic nano-domains within primary pyrite from this work (Fig. 3e, f), we suggest that fluid-mediated polymetallic melts and gold nanoparticle transport are both relevant to upgrading orogenic Au deposits. Where LMCE is absent from the system, then nanoparticle transport would become the dominant mechanism.

All aspects influencing the behavior of gold nanoparticles, their transport, and how they aggregate in different environments must be examined in detail if we want to better understand and resolve the processes that govern the formation of high-grade gold zones. However, many unanswered questions remain regarding nanoparticle processes in Au deposits, but discovering direct evidence for gold nanoparticles associated with Au remobilization in an Archean orogenic deposit serves to highlight that this mechanism is not restricted to a specific geologic time period or deposit setting. Future research should aim to: (1) understand the role of Ag in the behavior of gold nanoparticles because almost all natural gold contains significant Ag and many epithermal deposits are host to electrum (i.e., <80 wt.% Au, >20 wt.% Ag); (2) examine the nature of gold within precursor pyrite to

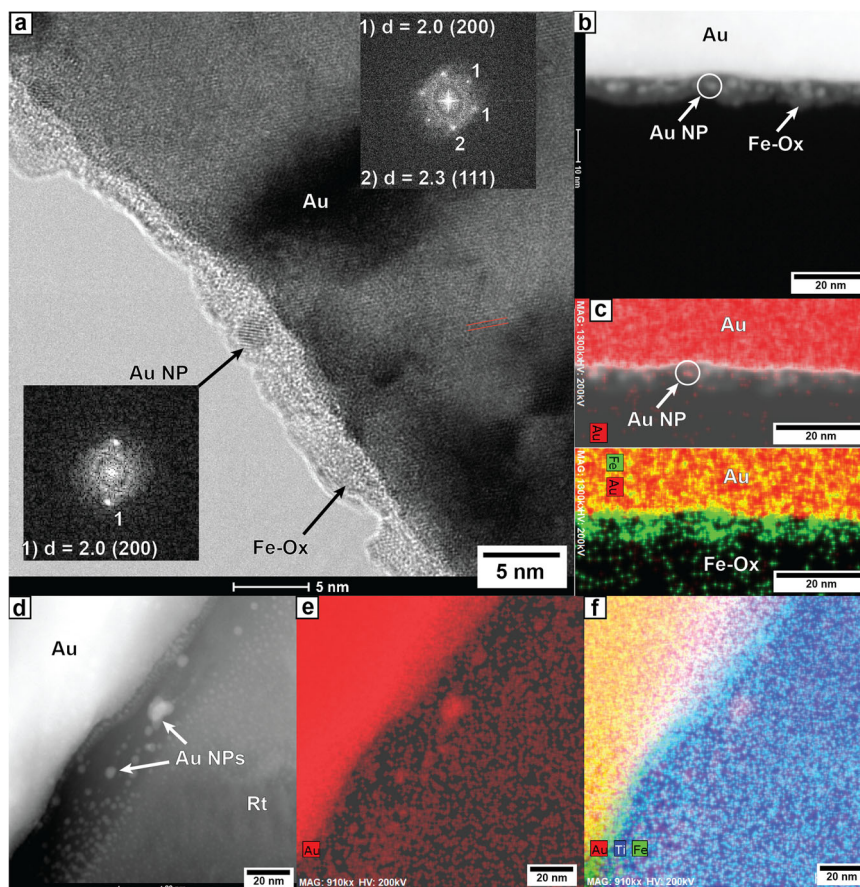


Fig. 6 High-resolution TEM image with fast Fourier transform (FFT) patterns, STEM images, and STEM-EDS elemental maps from locations shown in Fig. 4a. **a** High-resolution TEM image of Fe oxide on coarse gold surface with FFT patterns for gold nanoparticles and coarse gold. Numbers refer to FFT legend provided with FFT. **b** STEM image of Fe oxide and gold nanoparticles on coarse gold surface. **c** STEM-EDS elemental maps highlighting gold nanoparticles within Fe-oxides on the surface of coarse gold from **b**. Au is in red, Fe in green. **d** STEM image of gold nanoparticles within rutile at the margin of coarse gold-Fe oxide-rutile. **e-f**, STEM-EDS elemental maps highlighting gold nanoparticles within rutile. Au is in red, Fe in green, Ti in blue. Au gold, Fe, iron, Mag magnetite/maghemite, NP nanoparticle, Ox oxide, Rt rutile, Ti titanium. Some images have been cropped and rotated or reflected to produce similar orientations and aid comparison.

understand if there is a conversion of elemental Au to nanoparticles or simply nanoparticle liberation during dissolution; (3) clarify the relationship among gold nanoparticles and other elements, nanoparticles and minerals; and (4) determine the roles temperature and particle size play in the formation and aggregation of gold nanoparticles, specifically for conditions relevant to ore deposit formation.

Implications for Au deposits and relevant disciplines. High-grade, “bonanza-type” ore zones can form in ancient to recent Au deposit types owing to the transport and aggregation of gold nanoparticles^{5,6,8–10}. This mechanism can operate alone or in conjunction with fluid-mediated polymetallic melts to upgrade Au deposits. Dissolution of minerals, Au remobilization, counterion activity, and pH fluctuation are likely controls for gold nanoparticle formation, transport, and aggregation. The underlying mechanism for gold coarsening may, however, differ between orogenic (attachment, dissolution, and monomer transfer) and epithermal (diffusion-limited aggregation and orthokinetic aggregation)⁸ deposits. The existence of these different gold coarsening processes has far-reaching implications for other disciplines given that gold nanoparticle research is a critical component of material science^{40,41}, nanomedicine^{42,43}, and nanotechnology^{44,45}. A more complete understanding of natural gold nanoparticles and their interaction with other natural

materials may enhance laboratory manipulation for a variety of disciplines.

Methods

Geological sampling. Rock sampling and bedrock mapping was carried out by the lead author as an employee of the Ontario Geological Survey. The Universal Transverse Mercator (UTM) co-ordinates for the location of the sample used in this study are 378743 m E, 5299846 m N using NAD83 in zone 17. The sample location can also be seen with reference to the detailed outcrop map (Fig. 1b) and is shown by a yellow star.

SEM-EDS. This work was performed with a Zeiss EVO 50 SEM at the Geoscience Laboratories in Sudbury, ON, Canada. The SEM is equipped with an Oxford X-Max 50 mm² EDS, and used Oxford’s Aztec[®] software package. Operating conditions were 20 kV and ≈750 pA with variable counting times for each spot analysis (20–40 s) and used a working distance of 8.5 mm.

TEM of FIB sections. Extraction of FIB sections was conducted with an FEI Helios 650 NanoLab FIB at the 4D LABS at Simon Fraser University, Vancouver, BC, Canada. FIB sections were lifted with a platinum gas-glue and thinned with ion gas milling (Ga ions) to electron transparency. The FIB sections were analyzed with a field-emission TEM FEI Talos F200x at the Manitoba Institute for Materials, at the University of Manitoba, Winnipeg, Manitoba, Canada. Imaging in bright and dark-field mode was performed with an accelerating voltage of 200 kV and with a 16 MB ceta camera and a Fischione high angle annular dark-field detector. Compositional analysis was performed in STEM-EDS mode with four SDD detectors. Micro-scale phases were identified in the previous research⁴ and confirmed here at the nanoscale using a combination of Selected Area Electron Diffraction (SAED) and fast Fourier transform (FFT) patterns, chemical distribution maps, semi-

quantitative chemical analyses, and textural features of phases previously described in the literature. TEM and STEM-EDS chemical distribution maps were processed with the TEM Imaging & Analysis (a trademark of FEI) and Esprit 1 (a trademark of Bruker Nano).

Quality control during TEM-STEM examinations. TEM and STEM imaging can cause significant damage to the sample owing to beam-sample interactions. The two main damage types that samples experience are displacement effects and breaking of chemical bonds⁴⁶. Imaging in TEM and STEM mode can generate similar integrated doses and dose rates but in TEM mode, a defined area for the entire image is illuminated, whereas a smaller area of the sample is illuminated with a similar peak dose/rate in STEM mode than the larger area in TEM mode (during the same acquisition time)⁴⁶. Thus, an individual nanoparticle in, for example, a FIB section is exposed to a higher peak dose/rate in STEM than TEM mode.

In this study, the gold nanoparticles were exposed to the highest peak dose/rate during the recording of chemical distribution maps with STEM-EDS (maximum 30 min). For this reason, STEM images were recorded prior to and during the recording of STEM-EDS chemical distribution maps. In addition, TEM images were taken from the same area after the recording of the STEM-EDS chemical distribution maps. STEM and TEM images taken before, during, or after the recording of the chemical maps were then compared with identify potential damage to the samples. Besides the drift of the sample, especially detectable at high magnification, no changes in the number, morphology, and texture of any mineralogical feature were observed during the recording of the STEM-EDS chemical distribution maps.

Data availability

No data sets were generated or analyzed during this study.

Received: 24 April 2020; Accepted: 5 February 2021;

Published online: 11 March 2021

References

- Goldfarb, R. J. et al. Distribution, character, and genesis of gold deposits in metamorphic terranes. *Econ. Geol.* **100th Anniversary**, 407–450 (2005).
- Goldfarb, R. J. & Groves, D. I. Orogenic gold: common or evolving fluid through time. *Lithos* **233**, 2–26 (2015).
- Groves, D. I., Goldfarb, R. J., Gebre-Mariam, M., Hagemann, S. G. & Robert, F. Orogenic gold deposits: a proposed classification in the context of their crustal distribution and relationship to other gold deposit types. *Ore Geol. Rev.* **13**, 7–27 (1998).
- Hastie, E. C. G., Kontak, D. J. & Lafrance, B. Gold remobilization: insights from Au deposits in the Swayze greenstone belt, Abitibi Subprovince, Canada. *Econ. Geol.* **115**, 241–277 (2020).
- Voisey, C. R. et al. Aseismic refinement of orogenic gold systems. *Econ. Geol.* **115**, 33–50 (2020).
- Petrella, L. et al. Colloidal gold transport: a key to high-grade gold mineralization? *Miner. Deposita* **55**, 1247–1254 (2020).
- Williams-Jones, A. E., Bowell, R. J. & Migdisov, A. A. Gold in solution. *Elements* **5**, 281–287 (2009).
- Saunders, J. A. & Burke, M. Formation and aggregation of gold (electrum) nanoparticles in epithermal ores. *Minerals* **7**, 163–174 (2017).
- Gartman, A. et al. Boiling-induced formation of colloidal gold in black smoker hydrothermal fluids. *Geology* **46**, 39–42 (2018).
- Saunders, J. A. Colloidal transport of gold and silica in epithermal precious-metal systems: evidence from the Sleeper deposit, Nevada. *Geology* **18**, 757–760 (1990).
- Deditius, A. P. et al. Trace metal nanoparticles in pyrite. *Ore Geol. Rev.* **42**, 32–46 (2011).
- Palenik, C. S. et al. “Invisible” gold revealed: direct imaging of gold nanoparticles in a Carlin-type deposit. *Am. Mineral.* **89**, 1359–1366 (2004).
- Reich, M. et al. Thermal behavior of metal nanoparticles in geologic materials. *Geology* **34**, 1033–1036 (2006).
- Hough, R. M., Noble, R. R. P. & Reich, M. Natural gold nanoparticles. *Ore Geol. Rev.* **42**, 55–61 (2011).
- Ciobanu, C. L. et al. Gold-telluride nanoparticles revealed in arsenic-free pyrite. *Am. Mineral.* **97**, 1515–1518 (2012).
- Mercier-Langevin, P. et al. *Targeted Geoscience Initiative 5, Gold Project: a summary of contributions to the understanding of Canadian gold systems*; in Targeted Geoscience Initiative 5: Contributions to the Understanding of Canadian Gold Systems, (eds. Mercier-Langevin, P., Lawley, C. J. M., & Castonguay, S.) Geological Survey of Canada Open File 8712, 1–30 (2020).
- Monecke, T., Mercier-Langevin, P., Dubé, B. & Frieman, B. Geology of the Abitibi greenstone belt. *Rev. Econ. Geol.* **19**, 7–49 (2017).
- Katz, L. R., Kontak, D. J., Dubé, B. & McNicoll, V. The geology, petrology, and geochronology of the Archean Côté Gold large-tonnage, low-grade intrusion-related Au(-Cu) deposit, Swayze greenstone belt, Ontario, Canada. *Can. J. Earth Sci.* **54**, 173–202 (2017).
- Thompson, P. H. *A New Metamorphic Framework for Gold Exploration in the Timmins-Kirkland Lake Area, Western Abitibi Greenstone Belt: Discover Abitibi Initiative*. Ontario Geological Survey, Open File Report 6162, 1–104 (Ontario Geological Survey, 2005).
- Putnis, A. Mineral replacement reactions. *Rev. Mineral. Geochem.* **70**, 87–124 (2009).
- Tomkins, A. G. & Mavrogenes, J. A. Mobilization of gold as a polymetallic melt during Pelite Anatexis at the Challenger Deposit, South Australia: A metamorphosed Archean gold deposit. *Econ. Geol.* **97**, 1249–1271 (2002).
- Tomkins, A. G., Pattison, D. R. M. & Zaleski, E. The Hemlo gold deposit, Ontario: an example of melting and mobilization of a precious metal-sulfosal assemblage during amphibolite facies metamorphism and deformation. *Econ. Geol.* **99**, 1063–1084 (2004).
- Ciobanu, C. L., Birch, W. D., Cook, N. J., Pring, A. & Grundler, P. V. Petrogenetic significance of Au–Bi–Te–S associations: the example of Maldon, Central Victorian gold province, Australia. *Lithos* **116**, 1–17 (2010).
- Tooth, B., Ciobanu, C. L., Green, L., O’Neill, B. & Brugger, J. Bi-melt formation and gold scavenging from hydrothermal fluids: an experimental study. *Geochim. Cosmochim. Acta* **75**, 5423–5443 (2011). 2011.
- Zhou, H. et al. Nano- to micron-scale particulate gold hosted by magnetite: a product of gold scavenging by bismuth melts. *Econ. Geol.* **112**, 993–1010 (2017).
- Cabri, L. J. Phase relations in the Au–Ag–Te system and their mineralogical significance. *Econ. Geol.* **60**, 1569–1606 (1965).
- Capitani, G. Bizarre artefacts in transmission electron microscopy preparation and observation of geological samples. *Eur. J. Mineral.* **31**, 857–873 (2019).
- Hotze, E. M., Phenrat, T. & Lowry, G. V. Nanoparticle aggregation: challenges to understanding transport and reactivity in the environment. *J. Environ. Qual.* **39**, 1909–1924 (2010).
- Batista, C. A. S., Larson, R. G. & Kotov, N. A. Nonadditivity of nanoparticle interactions. *Science* **350**, 1242477 (2015).
- Boyle, R. W. *The geochemistry of gold and its deposits*. Geological Survey of Canada Bulletin 280, 1–584 (Geological Survey of Canada, 1979).
- Morrison, I. D. & Ross, S. *Colloidal dispersions: suspensions, emulsions and foams*. Wiley Interscience, 1–656 (Wiley Interscience, New York, 2002).
- Csapó, E. et al. Surface and structural properties of gold nanoparticles and their biofunctionalized derivatives in aqueous electrolytes solution. *J. Dispers. Sci. Technol.* **35**, 815–825 (2014).
- Kontonikas-Charos, A. et al. Feldspar evolution in the Roxby Downs granite, host to Fe-oxide Cu–Au–(U) mineralisation at Olympic Dam, South Australia. *Ore Geol. Rev.* **80**, 838–859 (2019).
- Nielsen, M. H. et al. Investigating processes of nanocrystal formation and transformation via liquid cell TEM. *Microsc. Microanal.* **20**, 425–436 (2014).
- De Yoreo, J. J. et al. Crystallization by particle attachment in synthetic, biogenic, and geologic environments. *Science* **349**, aaa6760 (2015).
- Becker, U., Reich, M. & Biswas, S. Nanoparticle-host interactions in natural systems; in *Nanoscope Approaches in Earth and Planetary Sciences*, (eds. Brenker, F. E., & Jordan G.) *European Mineralogical Union (EMU)* **8**, Chapter 8 (2010).
- Buffat, P. & Borel, J.-P. Size effect on the melting temperature of gold particles. *Phys. Rev. A* **13**, 2287–2298 (1976).
- Castro, T., Reifemberger, R., Choi, E. & Andres, R. P. Size-dependent melting temperature of individual nanometer-sized metallic clusters. *Phys. Rev. B* **42**, 8548–8556 (1990).
- Burda, C., Chen, X., Narayanan, R. & El-Sayed, M. A. Chemistry and properties of nanocrystals of different shapes. *Chem. Rev.* **105**, 1025–1102 (2005).
- El-Zoka, A. A., Howe, J. Y., Newman, R. C. & Perovic, D. D. In situ STEM/SEM study of the coarsening of nanoporous gold. *Acta Mater.* **162**, 67–77 (2019).
- Welborn, S. S. & Detsi, E. Small-angle X-ray scattering of nanoporous materials. *Nanoscale Horiz.* **5**, 12–24 (2020).
- Park, S. et al. Reversibly pH-responsive gold nanoparticles and their applications for photothermal cancer therapy. *Sci. Rep.* **9**, 20180 (2019).
- Sindhvani, S. et al. The entry of nanoparticles into solid tumours. *Nat. Mater.* **19**, 566–575 (2020).
- Chen, Y., Zhao, Y., Yoon, S. J., Gambhir, S. S. & Emelianov, S. Miniature gold nanorods for photoacoustic molecular imaging in the second near-infrared optical window. *Nat. Nanotechnol.* **14**, 465–472 (2019).
- Han, G. et al. Controlled fabrication of gold nanotip arrays by nanomolding-necking technology. *Nanotechnology* **31**, 144001 (2020).
- Nicholls, D. et al. Minimising damage in high resolution scanning transmission electron microscope images of nanoscale structures and processes. *Nanoscale* **12**, 21248 (2020).
- Ontario Geological Survey. 1:250 000 scale bedrock geology of Ontario. *Ontario Geological Survey Miscellaneous Release–Data 126–Revision 1* (2011).

48. Hastie, E. C. G., Lafrance, B. & Kontak, D. J. Observations on the Kenty and Rundle deposits, Swayze greenstone belt. *Ontario Geological Survey Open File Report 6313*, 9-1-9-9 (2015).

Acknowledgements

We acknowledge financial support offered by the Ontario Geological Survey (OGS) and the Goodman School of Mines at Laurentian University. This work constitutes part of a PhD thesis by the lead author that is supported through the Ontario Geological Survey-Laurentian University Graduate Mapping School Agreement. The project was also partially supported through NSERC grants to M.S. and D.J.K. Thank you to N. Thébaud and M. Reich for comments on the manuscript. Thanks to C. Mortimer and L. Salo for providing knowledge of the local terrain during field work. In addition, special thanks to the Royal Ontario Museum (ROM) for providing access to the high-grade Kenty gold specimen photographed. Finally, thanks to staff members at 4D LABS (Simon Fraser University), Manitoba Institute for Materials (University of Manitoba), and Geoscience Laboratories (Ontario Geological Survey) for technical support.

Author contributions

All authors jointly conceived the study. E.C.G.H. performed the field work, petrography, and SEM-EDS imaging and analyses. M.S. performed the TEM observations, analyses, and data processing. E.C.G.H. and M.S. interpreted the data with assistance from B.L. and D.J.K. B.L. and D.J.K. supervised the project. E.C.G.H. wrote the paper with contributions from all other authors.

Competing interests

The authors declare no competing interests.

Additional information

Supplementary information The online version contains supplementary material available at <https://doi.org/10.1038/s43247-021-00126-6>.

Correspondence and requests for materials should be addressed to E.C.G.H.

Peer review information Primary handling editor: Joe Aslin

Reprints and permission information is available at <http://www.nature.com/reprints>

Publisher's note Springer Nature remains neutral with regard to jurisdictional claims in published maps and institutional affiliations.



Open Access This article is licensed under a Creative Commons Attribution 4.0 International License, which permits use, sharing, adaptation, distribution and reproduction in any medium or format, as long as you give appropriate credit to the original author(s) and the source, provide a link to the Creative Commons license, and indicate if changes were made. The images or other third party material in this article are included in the article's Creative Commons license, unless indicated otherwise in a credit line to the material. If material is not included in the article's Creative Commons license and your intended use is not permitted by statutory regulation or exceeds the permitted use, you will need to obtain permission directly from the copyright holder. To view a copy of this license, visit <http://creativecommons.org/licenses/by/4.0/>.

© The Author(s) 2021